Phys. Status Solidi A **207**, No. 10, 2387–2394 (2010) / **DOI** 10.1002/pssa.201026206

physica status solidi a
www.pss-a.com
applications and materials science

Analysis of fluctuation processes in forward-biased solar cells using noise spectroscopy

Robert Macku* **and Pavel Koktavy****

Faculty of Electrical Engineering and Communication, Department of Physics, Brno University of Technology, Technicka 8, 616 00 Brno, Czech Republic

Received 4 March 2010, revised 15 April 2010, accepted 30 April 2010
Published online 4 June 2010

Keywords 1/*f* noise, non-destructive diagnostic, power spectral noise density, solar cells, transport mechanism

* Corresponding author: e-mail xmacku05@stud.feec.vutbr.cz, Phone: +420 541 143 277, Fax: +420 541 143 133
** e-mail koktavy@feec.vutbr.cz, Phone: +420 541 143 394, Fax: +420 541 143 133

The manufacturing technology of n^+p solar cells currently features a very high level of perfection. Its further development appears to be limited by amongst other issues imperfect diagnostic methods. The objective of our research consists in non-destructive studies of processes that influence specimen life and reliability. To this end, we are going to employ noise-based analysis methods. These methods are closely related to some specimen bulk imperfections, crystal-lattice-defect-induced traps, local-stress-subjected regions and, finally, breakdowns, which might bring about specimen destruction. Based on a detailed study and understanding of transport processes, regions in which noise is generated can be identified and appropriate technological measures can be proposed and adopted. Our research focuses, first of all, on the structures, which are inhomogeneous in their nature and are difficult to diagnose. On the basis of our experiments carried out to date, it has been established that the noise signal arises as a consequence of several concurrent processes. A noise model has been worked out and a mathematical description of separate noise source behaviour has been suggested. Our model includes the shot noise, the 1/*f* noise and a $1/f^2$ spectrum type noise and provides an account of the unconventional behaviour of solar cells.

1 Introduction In terms of cost reduction for photovoltaic systems the use of a new method for solar cells diagnostics is a very promising approach. Silicon based single junction solar cells are currently the most widespread production alternative. The major advantage of using silicon as a base material is the stray procedure of extended dimension in got production. The solar cell surface area is generally up to several hundred centimetres square. The *pn* junction is very close to the surface and it follows surface texturing. Due to this fact, the solar cell structure is very sensitive to surface damage and imperfections in the bulk of material. Our aim is above all characterization of the bulk imperfections or inhomogeneity and regions where it is situated. The low-frequency noise measurement of a typical solar cell is investigated in this paper. During our study we proved that the noise contributions of the solar cells are quite complicated. Their difficult character is probably the result of a large *pn* junction area and a great number of local defects. On this account, we carry out experiments with relatively small samples.

2 Experimental details It is typical of solar cells that the nature of the noise observed depends on the voltage applied to them. This can be attributed to variations in the transport mechanisms. This is why our study has been divided into two parts: first, the behaviour of forward-biased, and, second, that of reverse-biased *pn* junctions of solar cells. From a procedural viewpoint, the approach remains the same in both cases. The nature of noise will be appraised on the basis of measurements of the noise double-sided power spectral density (PSD). The PSD of a stationary noise signal $u(t)$ characterizes the distribution of signal noise power *versus* frequency. In our studies, we will track the current fluctuations. To this end, we will introduce the quantity $S_i(f)$. A simplified circuit diagram of our measurement set up is shown in Fig. 1.

The solar cell bias voltage is provided by a high-precision laboratory power supply. Its output voltage must be filtered because of the presence of additive noise types. The filter cut-off frequency is approximately 1 Hz. The specimen under investigation is placed in a dark environment, is

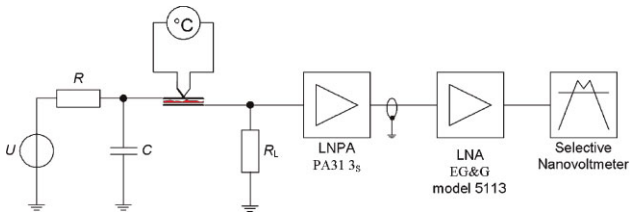

Figure 1 (online colour at: www.pss-a.com) Simplified circuit diagram of experimental arrangement for noise measurement. Here U is the bias voltage supply, LNPA is the low-noise pre-amplifier, and LNA is the low-noise amplifier.

electrically shielded and kept at a constant temperature $16.6 \pm 0.2\,^{\circ}\mathrm{C}$ to avoid self-heating. To measure the specimen current fluctuations, a pick-up resistor R_L is connected in series with the specimen ($R_L = 5.36\,\Omega$).

The noise voltage is amplified by means of low-noise amplifiers (PA31 – gain 20 dB, cut-off frequency 10 MHz; EG&G 5113 – gain 30 dB, cut-off frequency 1 MHz) and measured by means of a selective nanovoltmeter (Signal Recovery Model 7310), measuring the root-mean-square value of the noise signal in a narrow frequency band (defined by effective noise bandwidth – ENBW). The current fluctuation PSD is determined from the voltage fluctuations, where $S_u = (U_{rms}^2 - U_0^2)/\mathrm{ENBW}$ and $S_i = [(R_L + R_S)/R_L R_S]^2 \times S_u$ (applies to low-frequency fluctuation processes only). Here, U_{rms} is the narrow-band signal rms value, U_0 the noise background, R_S is the specimen resistance at a given operating point and ENBW is the effective noise bandwidth.

Figure 2 shows the behaviour of PSD at various forward-bias voltages applied to the specimen and experimental arrangement noise background. It is apparent that the noise power is inversely proportional to the frequency at very low-bias voltages, and directly proportional to the frequency squared at higher bias voltages. This indicates the presence of flicker noise ($1/f$ noise) and generation–recombination noise, which has a Lorentzian spectrum. At present, the cause of the noise, the noise type development behaviour, and, finally, the noise-type-switch-over bias, is not known. One of the tools to be used to elucidate this phenomenon will consist of measuring the UI characteristics. An example of such a plot in semilog representation is shown in Fig. 3. No observable breakdowns or other predominant effects, capable of affecting the measurement results undesirably, arise in the specimen under investigation. The UI curve has been subjected to an analysis and ideality factors n characterizing the current transport mechanisms have been determined. It is clear from Fig. 3 that several transport mechanisms are present in the solar cell in question. Therefore, a multiple-diode model may be introduced, in which several ideal diodes, each of them featuring only a single transport mechanism, are connected in parallel. Each of these diodes can be characterized by means of Shockley's equation with a particular transport coefficient n (ideality factor) and saturation current I_0. In a semilog plot, the above-mentioned different transport mechanisms are represented by linear segments and can be dealt with separately.

3 Transport characteristics of solar cells and transport process identification To express the specimen forward current I *versus* the applied voltage U plot, we will use Shockley's equation, which will be modified for our case:

$$I = I_0\left[\exp\left(\frac{e[U - R_s I]}{nkT}\right) - 1\right] + \frac{U - R_s I}{R_{sh}}, \qquad (1)$$

where n is the ideality factor, e the elementary charge, T the absolute temperature, k the Boltzmann's constant, R_s the specimen series resistance, and R_{sh} is the specimen leakage resistance. It is known that a generation–recombination

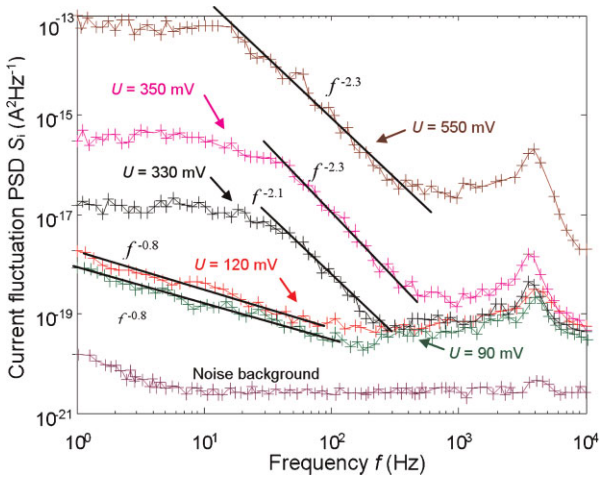

Figure 2 (online colour at: www.pss-a.com) Power spectral noise density of forward-biased solar cell for different bias voltages. Single crystal solar cell labelled K4, specimen temperature $T = 16.6 \pm 0.2\,^{\circ}\mathrm{C}$.

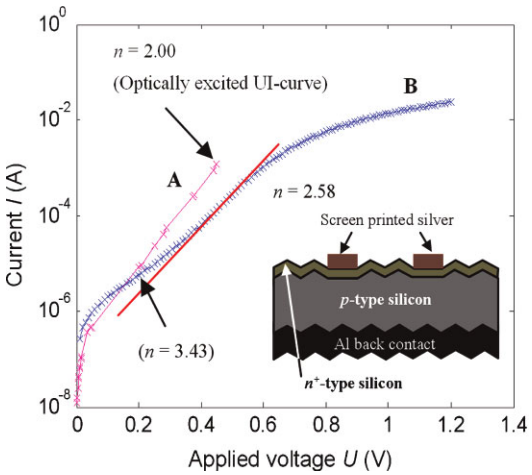

Figure 3 (online colour at: www.pss-a.com) Semilogarithmic current–voltage characteristic of forward-biased solar cells (electrically and optically excited), specimen K4, $T = 16.6 \pm 0.2\,^{\circ}\mathrm{C}$. Specimen area 276.3 mm^2.

process in the space charge region prevails for $n = 2$, whereas a diffusion process in the substrate of an n^+p solar cell prevails for $n = 1$ (in Eq. (1), the symbol U meaning the applied external voltage). It should be noted here that the saturation current also depends heavily on the transport process type. Formulas for both basic types have been derived and can be found in the literature (e.g. Ref. [1]). The principal question is, however, which transport mechanisms play a role here.

Our experiments show that the specimen current depends strongly on the temperature and that thus charge carrier tunnelling can be excluded. The values of n obtained from our solar cells do not correspond to 'traditional' values, which could mean either that the 'traditional' transport mechanisms (generation–recombination process, diffusion process) are not present here, or that these 'traditional' mechanisms are affected by another disturbing process. Several authors dealing with large-area *pn* junctions point out the effect of series resistance. It is stated in Ref. [2] that the finger contacts of solar cells cause lateral current densities in the n^+ layer (distributed series resistance). This in turn brings about considerable voltage drops in the case of large currents. The voltage over the junction directly under the contacts exceeds that between the contact couple. Therefore, the electric field intensity under the contacts is higher and the junction effective area is reduced (the term 'effective area' is used to express the shallow *pn* junction area enlargement in consequence of the surface texture). Consequently, the UI characteristics are distorted in this case and the transport coefficient values are higher than expected.

Another factor, which could substantially affect the measurement results, is the leakage resistance value. It is generally assumed that the leakage resistance (being modelled as a resistance which is connected in parallel to the *pn* junction) is sufficiently large for its effect to be ignored or not observable. A simulation on the basis of Eq. (1) has been carried out, in which the diffusion process, the leakage resistance R_{sh} and, in addition, the series resistance R_s have been included into the considerations. The result is shown in Fig. 4.

It can be said that the segment of the *U–I* curve, which is distorted by the action of the leakage resistance can be considered as linear. The initial curvature can be found in the curve B of Fig. 3, too. We may therefore assume that the effect of the leakage resistance is predominant at forward voltages U below about 300 mV (see Fig. 3); the generation–recombination-controlled conductivity process ($n = 2.58$, higher value of the coefficient being due to the distributed series resistance) contribution increase is observed at forward voltages of up about 620 mV (see Fig. 3). Above this voltage, the characteristic is deformed due to the macroscopic effect of the series resistance and overlaps the diffusion process region.

The influence of the distributed series resistance on the shape of the *U–I* can be proved by measuring the *U–I* characteristic of a solar cell which is irradiated by monochromatic light of various intensities E. The short-circuit current I_{sc} equals the photocurrent generated, whereas the open-circuit voltage U_{oc} corresponds to the cell being powered by a voltage source while excluding the effect of the series resistance (plots of $I_{sc} = f(E)$ and $U_{oc} = f(E)$ will be measured and, subsequently, the *U–I* curve will be plotted). For more detailed information, see, e.g. in Ref. [2]. These measurements were also carried out. The result is shown in Fig. 3, curve A. It is seen that the transport mechanism does correspond to the generation–recombination process ($n = 2.00$). At the same time, the leakage resistance decreased.

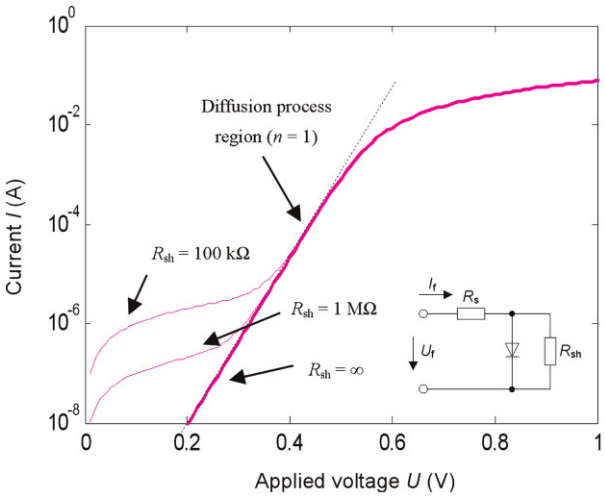

Figure 4 (online colour at: www.pss-a.com) Simulation of current–voltage characteristic of an ideal *pn* junction diode with different shunt resistances R_{sh} and constant series resistance $R_s = 1\,\Omega$, $T = 300$ K.

Another piece of information which has to be obtained from experimental data set (Fig. 3 curve B) is the magnitude of the saturation current, leakage resistance and series resistance. It can be read out from the plot using least squares curve fitting based on Eq. (1). We use the Matlab computing environment with Curve Fitting Toolbox and Levenberg–Marquardt minimizing algorithm.

Taking into account the identified generation–recombination transport process we obtain the following parameters for specimen K4. Parallel leakage resistance, $R_{sh} \approx 44.4\,\text{k}\Omega$, macroscopic series resistance (its effect is apparent, above all, in Fig. 3 – curvature of B-characteristic in high-current region) its magnitude being approximately $R_s \approx 3.2\,\Omega$ and finally the saturation current is $I_{0(g-r)} = 2.7 \times 10^{-7}$ A.

4 Noise types observed in solar cells

4.1 1/*f* noise in semiconductors It has been shown during many years of noise research that 1/*f* noise is closely related to the specimen bulk homogeneity being impaired, for example, by the presence of impurities or defects in the crystal lattice [3]. To improve the device reliability and service life, it is therefore necessary to minimize this kind of noise. This is why it is essential to understand the causes of the 1/*f* type noise origin. In 1970, Van der Ziel published a detailed treatise on 1/*f* noise in semiconductors and also dealt

with some problems connected with the description of *pn* junctions (see Ref. [4]). It is to be noted that 1/*f* noise is still a central problem to be solved in fluctuation physics. Our research and a proposal for the solar cell behaviour will be based on a generalized Hooge's model. According to Hooge's, this type of noise arises as a result of resistance fluctuations in the semiconductor bulk. For homogeneous layers, the Hooge's empirical formula reads as follows [5]:

$$\frac{S_i(f)}{I^2} = \frac{S_R(f)}{R^2} = \frac{\alpha_H}{fN}. \tag{2}$$

Here, $S_i(f)$ is the PSD related to current fluctuations, $S_R(f)$ the PSD related to resistance fluctuations, f the frequency, N the number of free charge carriers in the semiconductor and, finally, a_H is a dimensionless constant, called Hooge's constant. Equation (2) is purely empirical. The only assumption having been applied here requires the behaviour of individual electrons not to influence and not to be influenced by other electrons.

As the resistance of a semiconductor is inversely proportional to the product of the charge carrier number N and mobility μ ($R = L^2/e\mu N$, L is the specimen length) [4], there are two possible sources of fluctuations. One of them is the mobility μ, and the other the number of free charge carriers N. As we are looking for the fluctuations of the resistance R, the fluctuating resistor must be connected in parallel to a voltage source for current fluctuations to take place.

It is to be noted that considerations related to homogeneous semiconductor layers cannot be applied if the free charge carrier concentration depends on the coordinate, $n = n(x)$ and $p = p(x)$. However, this is just the case of the *pn* junction in the solar cell structure. Therefore, the well-established theoretical approach and Eq. (2) cannot be applied. In 1977, Kleinpenning [6] published calculations related to *pn* junctions of various geometries. We are going to apply the conclusions of his paper here. Let us consider a *pn* junction of our solar cell, which can be labelled as a so-called long *pn* junction (with respect to the diffusion length). If the junction is forward-biased the number of carriers grows when increasing the voltage across the diode. The applied voltage can be understood to be a source of excess generation. A new equilibrium state will be established in the semiconductor after a certain time has elapsed. It holds that $np = \text{constant}$ and $np > n_0^2$ (n_0 is the intrinsic concentration). In this way, the total number of free charge carriers and its dependence on the current is determined. This means that the assumption has been made that this type of noise is due to fluctuations in charge carrier mobility rather than concentration fluctuations. According to Ref. [6], this has only been proved experimentally on silicon *pn* junctions. In his paper, Kleinpenning gives Eq. (3) for the PSD of current fluctuations 1/*f* for a silicon diode (modified for a long *pn* junction). We would like to note that this formula has also been derived independently of Kleinpenning's paper in the course of our research. However, a detailed derivation of the formula will not be dealt with here. Therefore, it holds

$$S_i = \frac{\alpha_H \gamma e I^2}{(I + I_0)\tau_\alpha f}. \tag{3}$$

Here, γ is a numeric constant depending on the type of transport process in the specimen, τ_α the lifetime, which in turn depends on the transport process type, I_0 the saturation current, e the elementary charge and f is the measuring frequency. The variable α_H has the same meaning as in Eq. (2). The transport process type is the key information entered in the following theoretical considerations. From the considerations made in the preceding paragraph, we already know that the generation–recombination process takes place in the space charge region, for which case the constant γ of Eq. (3) equals 2/3 (1/4 for a substrate diffusion process). Its meaning results from the derivation, but we are not going to deal with it here. What remains to be carried out is the determination of the lifetime τ_α. Formulas for both basic cases have been derived and can be found in the literature (e.g. in Ref. [1]). It holds for the generation–recombination process:

$$I_{0(g-r)} = \frac{A_{pn} e n_i d}{\tau_\alpha}. \tag{4}$$

Here, A_{pn} denotes the junction area, n_i the intrinsic concentration, and d is the depletion region width. The cell surface area has to be determined macroscopically and the junction area has to be additionally enlarged because of the surface pyramidal texture [7]. The K4 specimen area is 189.3 mm^2 and the junction area $A_{pn} = 276.3$ mm^2. For more information, see Ref. [7]. The intrinsic concentrations *versus* temperature plots are tabulated for silicon. For a temperature of 16.6 °C (289.75 K) it equals $n_i = 8 \times 10^8$ cm^{-3}. The depletion region width d will be determined indirectly by calculation from Eq. (5).

$$U_B \approx \frac{e N_A d^2}{2\varepsilon_0 \varepsilon_r} \quad \rightarrow \quad d = \left(\frac{2\varepsilon_0 \varepsilon_r U_B}{e N_A} \right)^{1/2}. \tag{5}$$

Equation (5) can be found for example in Ref. [1]. It is based on the reverse-biased junction CU characteristics measured. When measuring these characteristics, we found the concentration profile of the solar cell junction to be near that of an abrupt junction. In this case, a one-sided junction approximation can be used, in which case the depleted part of the n^+ type semiconductor is neglected and Eq. (5) holds. The voltage across the barrier equals the sum of an external U_{VN} and a diffusion voltage U_{DIF}, which is in the K4 specimen equal to 0.497 V. Another important parameter is the acceptor concentration (proportional to the slope of the measured CU characteristic). Dynamic capacitance was considered; the acceptor concentration therefore is $N_A = 5.85 \times 10^{21}$ m^{-3}. For more information, see, e.g. Ref. [7]. Combining Eqs. (4) and (5) we get the junction carrier effective lifetime $\tau_\alpha = 8.99 \times 10^{-9}$ s. We have also determined experimentally the lifetime of minority carriers

(electrons) in the substrate using the open circuit voltage decay (OCVD) method. This is a value valid throughout the substrate bulk. For the K4 specimen, the lifetime is $\tau_n = 1.25 \times 10^{-6}$ s. This value is substantially higher than that determined for the carriers in the junction and had to be used in the case of minority carrier diffusion in the substrate. The question arises here of, whether or not the 1/*f* noise can be evaluated or modelled in the above way in the specimens in which the series resistances play an important role (IV curve compression) and we cannot be sure whether carrier diffusion transport is taking place here or not. Let us assume a lifetime ratio τ_n/τ_α, which equals about 140 for our specimen. This means that even if the diffusion process is predominant in the carrier transport, noise will be predominantly generated by the recombination process.

These considerations can be further extended by including the effect of the leakage resistance. In the above diode model of a solar cell (see Fig. 4) this is equivalent to the fact that a leakage resistance current has to be deducted from the *pn* junction current. Its effect is essential in the case of small forward currents, especially if we take into account the fact that the leakage resistance R_{sh} is equal to 44.4 kΩ only. Formula (3) has therefore to be modified and it holds

$$S_i = \frac{\alpha_H \gamma e (I - U_f/R_{sh})^2}{(I - U_f/R_{sh} + I_0)\tau_\alpha f}. \quad (6)$$

4.2 Analysis of the current dependence of the power spectral density To verify the correctness of our considerations, we will employ the PSD *versus* specimen current plot at a constant centre frequency. The measurement result is shown in Fig. 5.

It follows from Eq. (3) that the PSD of the 1/*f* type for $I < I_{0,\lambda}$ is directly proportional to the current squared and for $I > I_{0,\lambda}$ is directly proportional to the current (λ labels the transport process type). Nevertheless, the measurement result shown in Fig. 5 is very surprising. A sharp break in the characteristic slope is evident at the current $I = 1.94 \times 10^{-6}$ A and the forward voltage $U_f = 90$ mV. Moreover, the trend of the S_i *versus* the current *I* plot is exactly the opposite of what was expected.

It is also interesting to note that there is no perceivable change in the characteristic of Fig. 5 at the voltage at which the *g–r* process becomes predominant (approximately 300 mV in Fig. 3, curve B) and, simultaneously, a perceivable noise spectrum nature occurs, see Fig. 1). On the contrary, there is a marked deviation in the region of large currents, where the macroscopically observable series resistance also affects the UI characteristic. Several authors deal with the contacts, their influence and related noise. For example, paper [3] states that the noise generated by the *pn* junction is no longer predominant in the extremely high current region; instead, a noise contribution of a macroscopic series resistance R_s takes effect in compliance with Eq. (2). In this case, 1/*f* type noise is assumed to arise, for the PSD of which it holds: $S_i = \alpha_H I^2/fN_{eff}$, [8]. Here, N_{eff} denotes the effective number of free charge carriers in the contact region with a strong electric field. It is also apparent that the noise contribution is proportional to the specimen current squared. When carrying out the analysis, the carrier low-injection condition must be satisfied. Therefore, we are not going to deal with large-current regions.

A partial explanation of S_i *versus* *I* behaviour can be obtained from Eq. (6). Evaluation of the spectral density *versus* current plot is difficult to carry out now, because the specimen current and the voltage across the specimen are not directly proportional to each other. This is why a simulation (see Fig. 6) has been carried out to show the spectral density *versus* current plots.

Curve B corresponds to the expected behaviour according to Eq. (6), whereas the dotted line, starting from the

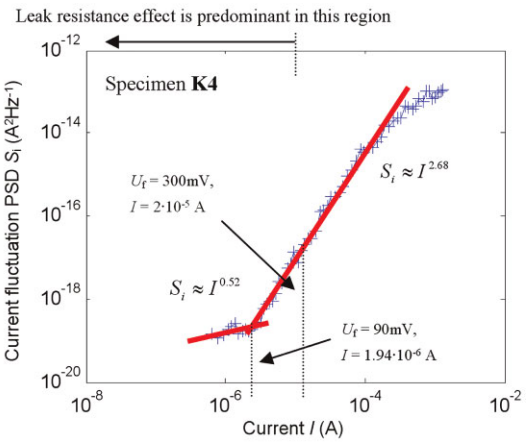

Figure 5 (online colour at: www.pss-a.com) Noise PSD as a function of current, $T = 16.7 \pm 0.2$ °C, centre frequency 10 Hz and ENBW = 1.6 Hz.

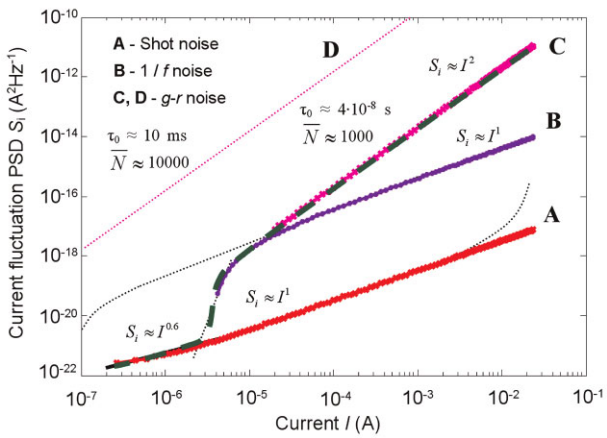

Figure 6 (online colour at: www.pss-a.com) Simulation of noise power spectral densities as a function of current through the solar cell, $T = 16.7$ °C, centre frequency 10 Hz, Hooge's constant $\alpha_H = 1 \times 10^{-3}$. The thick dashed line (green) represents the sum of individual noise components.

above-mentioned curve B, matches Eq. (3). In both curves, a region of $S_i \approx I^1$ (large current region assumed) evidently exists. The dotted line also includes a current-squared region ($I < I_{0,\lambda}$). However, this is not the case of curve B. Here the characteristic break region is found at substantially higher currents and the noise power contribution decreases approximately with the eighth power of the specimen current. Therefore 1/*f* type noise cannot be observed in the low-current region.

4.3 Shot noise Let us put another question now. If it has been proved that *1/f* noise is observed in the specimen (Fig. 1) and that it is possible for its spectral density to be directly proportional to the specimen current for $I > I_{0,\lambda}$ and to fall rapidly down to negligibly low-levels for $I < I_{0,\lambda}$ what is the kind of noise of Fig. 5. To make the spectral density grow proportionally to $I^{0.52}$? Extensive studies of conceivable alternatives have led us to shot noise. For a more detailed treatise of shot noise, see, e.g. Refs. [3, 9].

Let us have a look at what the shot noise will be like in the case of *pn* junctions. Our objective is to focus on the region of relatively low-forward currents. Although forward-biased, the *pn* junction still behaves as a potential barrier in the low-current region. Several different approaches can be found in the literature [3, 9]. Roughly speaking, the *pn* junction current results from the minority carrier injection. In noise considerations, both the diffusion and the generation and recombination of minority carriers must be taken into account. Another approach is based on the shot noise origin mechanism description, in which individual charge carrier passages over the potential barrier are observed and taken as mutually independent. In his paper [4], Albert Van der Ziel shows that these two approaches are equivalent. Quite another approach is suggested in Ref. [9]. It is not related to any noise origin mechanism. However, it provides good results. It is assumed in this approach that there are independent current sources and that the superposition principle applies to the current mean values. Furthermore, it is assumed that the *pn* junction current follows Eq. (1). Neglecting the series resistance effect, we get Eq. (7).

$$I = I_0\left(\mathrm{e}^{\frac{eU}{nkT}} - 1\right) + \frac{U}{R_{\mathrm{sh}}} = I_0\mathrm{e}^{\frac{eU}{nkT}} - I_0 + \frac{U}{R_{\mathrm{sh}}}\cdot \tag{7}$$

The current can be divided into a couple of independent noise generating contributions and another term that does not contribute any additional noise. This component corresponds to the leakage resistance current, which means that the current does not pass over any potential barrier. Assuming the noise source fluctuation mean values to be additive, we may use Eq. (7) to obtain the total PSD

$$S_i = \frac{\overline{I_{\mathrm{c}}{}^2(t)}}{\Delta f} = 2eI_0\mathrm{e}^{\frac{eU}{nkT}} + 2eI_0\cdot \tag{8}$$

Here, $I_{\mathrm{c}}^2(t)$ denotes the root-mean-square value of the current fluctuation and Δf is the bandwidth. A simulation of the PSD *versus* the specimen current plot was carried out in accordance with Eq. (8). The result is shown as curve A in Fig. 6. As the relation between the specimen voltage and current is not quite obvious, as in the 1/*f* noise simulation case, the K4 specimen UI characteristic has been employed for the simulation. The simulation provides interesting conclusions again. One of them is that it cannot be said generally for the *pn* junction that shot noise is directly proportional to the current, as is usual. Moreover, the curve shape can be influenced by the presence of series resistance, which is shown by a dotted line in Fig. 6. Shot noise is predominant in the region where 1/*f* noise is not important. The initial segment of the red line can be fitted by a straight line. This being done, the PSD is found to follow an $I^{0.6}$ – type function. This is in very good agreement with the measurement results. In the high-current region, the shot noise level is far below that of 1/*f* noise and can therefore be ignored.

4.4 Forward current region in which $1/f^2$ noise occurs It is our task in this paragraph to find a method of characterizing the noise process, the onset of which can be observed starting from the point at which the *g–r* process begins to be predominant (see Figs. 2,3 and 5), i.e. from approximately 300 mV upwards. This process is known to have a Lorentzian spectrum and a PSD increasing approximately with the current square. This is typical of generation–recombination noise (hereinafter, the G–R noise).

In general, G–R noise is considered to result from statistical fluctuations of charge carriers in consequence of charge carrier *generation*, *recombination*, random *capture and release* at the trap level in a semiconductor. Here, the trap levels in the gap play a role, being present due to various defects and impurities in the semiconductor bulk as well as in its surface. For more information, see, e.g. Ref. [9]. The following equation can be used to express the current fluctuation spectral density:

$$S_i = \frac{\overline{i_{\mathrm{n}}^2}}{\Delta f} = \frac{4\overline{I}^2\tau_0}{\overline{N}(1+\omega^2\tau_0{}^2)}\cdot \tag{9}$$

Here, i_{n}^2 is the root-mean-square value of the current fluctuations, Δf the frequency interval under investigation, $\overline{I}$ the current mean value (DC value), $\overline{N}$ the mean number of charge carriers and τ_0 is the effective time constant of charge carriers. The lowest-time-constant process will take the strongest effect.

Figure 7 shows the measured spectrum fit by Eq. (9) In this way, parameters of this function have been obtained, namely, the mean number of charge carriers $\overline{N} = 10\,000$ and the predominant time constant $\tau_0 = 10$ ms. Let us return to the plots of Figs. 5 and 6. The spectral density *versus* current plot simulation can be carried out here as well. To this end, we will employ the parameters obtained by approximation (see Fig. 7). The PSD is directly proportional to the current square, which is OK, but this type of noise is becoming heavily predominant in the low-current region, too. It means

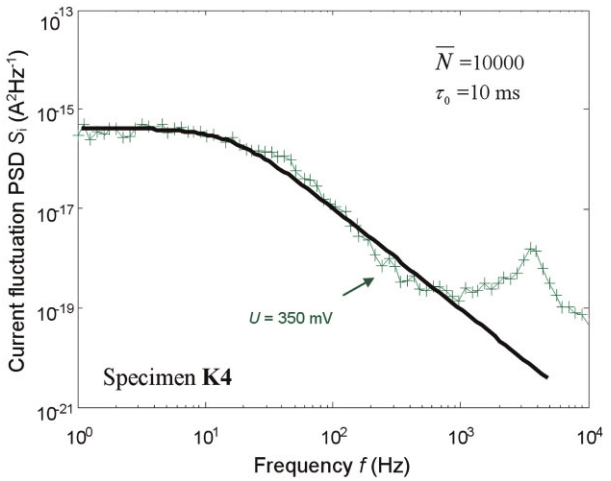

Figure 7 (online colour at: www.pss-a.com) Approximation of noise PSD by Eq. (9). Forward voltage $U_f = 350\,\text{mV}$, $T = 16.6 \pm 0.2\,^{\circ}\text{C}$.

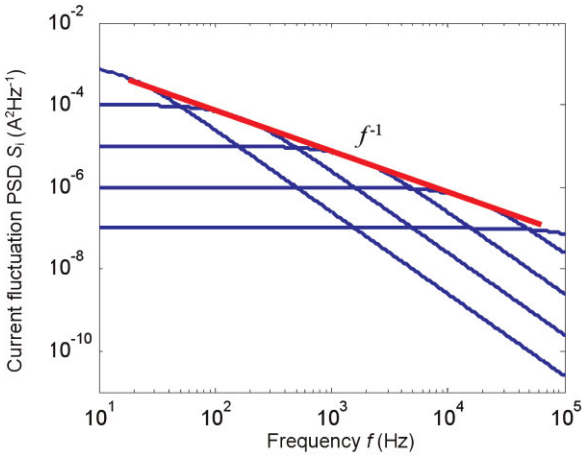

Figure 8 (online colour at: www.pss-a.com) 1/*f* noise origin model based on sum of Lorentzian spectrum. Time constants are in the range of 10^{-7} to 10^{-3} s.

that other types of noise could not be observed. If we carry out the approximation (extrapolation) of the function of Fig. 5, we will get quite different parameter values. They will be as follows: the time constant $\tau_0 = 4 \times 10^{-8}$ s and the mean number of charge carriers $\overline{N} = 1000$. The result of this simulation is represented by curve C in Fig. 6. The conclusion of this simulation is quite surprising: the time constant is in very good agreement with the carrier lifetime in the *pn* junction ($\tau_\alpha = 8.99 \times 10^{-9}$ s).

The following question must therefore be asked: Which type of noise, however different from the G–R noise, has a Lorentzian spectrum in the given frequency interval? And, additionally, which type of noise features the spectral density *versus* current plot and obeys, at least approximately, the square-law function? Moreover, the fluctuation process time constant should coincide with the charge carrier life in the *pn* junction. This inferential evidence hints at a very interesting fact. It may be said that there is the same fluctuation mechanism as in the 1/*f* noise here.

Let us consider a model for the generation of 1/*f* noise. It is known generally that if there are several mutually independent processes in a specimen which have Lorentzian spectral densities, 1/*f* noise will be observed in the given frequency interval. It holds

$$S_{1/f}(f) = \sum_i \overline{(\Delta N_i)^2} \frac{4\tau_i}{1+\omega^2\tau_i^2}\,. \tag{10}$$

Here, $S_{1/f}(f)$ is the PSD of 1/*f* noise, ΔN_i the charge carrier concentration fluctuation, τ_i the time constant of each process, and ω is the angular frequency. For more detailed information, see Ref. [9]. A model of 1/*f* noise generation is shown in Fig. 8.

One of the essential requirements for the above model and Eq. (10) to be applicable is that the different fluctuation processes must not interact with each other. If there were interactions, Lorentzian noise rather than 1/*f* noise would be obtained – see Ref. [10]. We may conclude as follows: The $1/f^2$ noise, as observed in our experiments, is caused by the same processes as 1/*f* noise. The difference as against the 1/*f* noise is that the individual processes influence each other at higher forward voltages. Therefore, considerations which are used to explain the G–R noise, where individual, mutually independent processes are assumed, cannot be used here. Instead, the sum of a multitude of processes and their noise contributions must be taken into account.

5 Results, discussion and conclusion The motivation of our research was to provide an explanation of non-standard noise properties of solar cells, which appears to be the central problem of noise-based non-destructive diagnostic methods. A number of experiments and measurements have been carried out on the basis of which an analysis and identification of observed noise contributions have been carried out. Proposed noise sources have been discussed. Simulation of their behaviour, i.e. spectral density *versus* current dependence, has been carried out. These spectral-density-*versus*-current plots proved to be very useful tools for analysing different types of noise. Note that the confrontation was carried out for several technologically identical specimens (not published here). In general, the simulated noise PSD and measured PSD may be by several orders of magnitude lower. The cause of the measured PSD exceeding in magnitude that resulting from theory may consist in the existence of inhomogeneities in the *pn* junction [3]. The larger the deviation, the poorer the junction homogeneity that can be expected.

The entire issue, i.e. the identification of processes determining the overall behaviour of the specimens, is rather complicated. What is observed as noise of solar cells appears to result from the concurrence of three partial noise processes, namely, shot noise, 1/*f* noise and $1/f^2$ spectrum type noise. Moreover, the specimen current *versus* applied voltage plot is heavily non-linear, which in turn aggravates

the complexity of the situation. The charge carrier transport mechanisms are difficult to identify in solar cells, although they are of key importance for any noise source mechanism suggestions. Observed experimental data deviation may be due, to a large extent, to the distributed series resistance. This issue has been paid much attention in our research. The correctness of our approach has been confirmed by *U–I* characteristic measurement of optically excited solar cells.

A very interesting conclusion of our studies is that the $1/f$ noise we have observed arises in the course of the charge carrier generation–recombination process in the depleted region of the solar cell. Moreover, it can be stated that the mutual independence of charge carrier fluctuation inducing processes is maintained at voltages of up to about 300 mV. The lifetime ratio τ_n/τ_α equals approximately 140 for our specimen. It means that even if the *U–I* characteristics are affected by the series resistance and the diffusion process is not apparent we may be for sure that – up to a certain point – the noise remains the result of recombination processes. Noise of the $1/f^2$ – type is observed at forward voltages over 300 mV. However, this is not the usually anticipated G–R noise. This type of noise arises from interactions between the fluctuation processes which formerly gave rise to the $1/f$ noise.

Acknowledgements This research has been supported by the Grant Agency of the Czech Republic within the framework of the project GAČR P102/10/2013 'Fluctuation processes in *pn* junctions of solar cells' and the research intention MSM 0021630503. This support is gratefully acknowledged.

References

[1] S. M. Sze, Physics of Semiconductor Devices (John Wiley & Sons, New York, 2006), ISBN 978-0-471-14323-9.
[2] M. Wolf and H. Rauschenbach, Adv. Energy Conversion **3**, 455–479 (1963).
[3] L. K. J. Vandamme, IEEE Trans. Electron Devices **41**, 11 (1994).
[4] A. Van Der Ziel, Noise: Sources, Characterization, Measurements (Prentice-Hall, Englewood Cliffs, New Jersey, 1970).
[5] F. N. Hooge, Physica **60**, 130 (1972).
[6] T. G. M. Kleinpenning, Physica **98b**, 141–151 (1977).
[7] R. Macku, P. Koktavy, and P. Skarvada, WSEAS Trans. Electron. **4**(9), 192–197 (2008).
[8] L. K. J. Vandamme, R. Alabedra, and M. Zommiti, Solid State Electron. **26**(7), 671–674 (1983).
[9] R. M. Howard, Principles of Random Signal Analysis and Low Noise Design (Wiley & Sons, Inc., New York, 2002), ISBN 0-471-22617-3.
[10] S. Mohammadi and D. Pavlis, IEEE Trans. Electron Devices **47**, 11 (2000).

